Development of a material model for AA7075 aluminium hot stamping

D'amours, G.; Ilinich, A.

Publisher's version / Version de l'éditeur:
https://doi.org/10.1088/1742-6596/1063/1/012033
Journal of Physics: Conference Series, 1063, 2018-07-01

IOP Conf. Series: Journal of Physics: Conf. Series **1063** (2018) 012033 doi:10.1088/1742-6596/1063/1/012033

Development of a material model for AA7075 aluminium hot stamping

G D'Amours[1] **and A Ilinich**[2]

[1] National Research Council Canada, Aluminium Technology Centre, Saguenay, Québec, Canada
[2] Ford Research and Innovation Center, Dearborn, Michigan, USA

Guillaume.Damours@cnrc-nrc.gc.ca, ailinich@ford.com

Abstract. This paper presents the development and validation of a material model for finite element analysis of aluminium hot stamping. It is based on Hill'48 yield function with a non-associated flow rule and isotropic, temperature and rate sensitive hardening. The model also includes phenomenological damage treatment which was developed for plastic instability and fracture prediction in non-isothermal conditions. A special attention was given to the calibration of thermal conductance. Validation was performed with a series of cross die hot stamping tests with in-situ temperature measurements.

1. Introduction

Auto manufacturers can improve fuel economy by decreasing the weight of their vehicles. The high strength AA7075 aluminium sheet is an attractive lightweight material for automotive applications due to its high specific strength in T6 or T73 tempers. However, its usage is still very limited partially due to poor room temperature formability. Elevating temperature of the sheet prior to forming is a possible solution to this problem as it leads to an increase in material ductility and a decrease in flow stress. In hot forming, the sheet is solutionized (i.e. heated above the solvus temperature) before the stamping operation. The process is carried out in non-isothermal conditions where die is cooled to almost room temperature. In recent years, researchers such as Harrison *et al.* [1], Ilinich *et al.* [2], Xiao *et al.* [3] and Kumar *et al.* [4] have started to work on this process and have formed high strength prototype parts with AA7000 series aluminium alloys.

Manufacturing of complex parts require finite element analysis to avoid trials and prototyping which is expensive and time consuming. Modeling elevated temperature forming is more complicated than conventional stamping. The finite element software LS-DYNA has some plane stress material models applicable for non-isothermal forming. However, there are no general stress state models available for solid elements that can describe aluminium anisotropy and support temperature and rate dependant hardening. For damage, LS-DYNA has a phenomenological damage accumulation model capable to predict both plastic instability and fracture. However, its current implementation is limited to isothermal conditions. Therefore, new models are necessary for the finite element analysis of the aluminium hot stamping process that take into account evolution of anisotropy, strain hardening and damage of aluminium sheets due to variations of temperature, strain rate and loading path observed with this process.

Among different parameters required for finite element analysis, the interfacial contact heat transfer conductance (HTC) plays a critical role by controlling the heat transfer from the blank to the tools. The

HTC in aluminium hot stamping have been investigated by Ilinich *et al.* [2] and Liu *et al.* [5]. Ilinich *et al.* [4] studied the effects of initial blank temperature, initial tool temperature, and contact pressure on the maximum HTC. Liu *et al.* [5] developed an inverse HTC determination technique using test results obtained with a Gleeble machine. While the prior research provides good staring values for HTC, it is still very important to perform HTC calibration for the particular physical setup and modeling method due to sensitivity of the results to a number of additional physical and modelling parameters.

This paper presents an overview of a plasticity and damage models developed for aluminium hot stamping. The calibration of the contact thermal conductance was performed by in-situ blank temperature measurements during cross die hot stamping and inverse modeling of the heat transfer.

2. Plasticity model

A plasticity model based on the non-associated plastic flow rule (non-AFR) with isotropic hardening was selected in this study due to its simplicity and flexibility. In this model, the plastic potential Q and the yield surface F were defined by two separate functions. The non-AFR models with simple Q and F functions are in many cases less computationally expensive than more complex AFR models yet capture complex anisotropic behavior equally well or better. These models can be calibrated with just tensile tests and are suitable for 3D solid elements.

Hill 1948 yield function [6] was used for both the plastic potential function Q and the yield surface function F. The yield surface F for 3D solid elements was of the following form:

$$F = F_{\mathrm{y}}(\sigma_{22}-\sigma_{33})^2 + G_{\mathrm{y}}(\sigma_{33}-\sigma_{11})^2 + H_{\mathrm{y}}(\sigma_{11}-\sigma_{22})^2 + 2L_{\mathrm{y}}{\sigma_{23}}^2 + 2M_{\mathrm{y}}{\sigma_{31}}^2 + 2N_{\mathrm{y}}{\sigma_{12}}^2 - {S_{\mathrm{y}}}^2 \quad (1)$$

where σ_{ij} are components of the stress tensor. F_{y}, G_{y}, H_{y}, N_{y}, L_{y} and M_{y} are the six coefficients of the Hill surface. To include planar stress anisotropy, stress anisotropy parameters σ_0, σ_{45} and σ_{90} were used to determine F_{y}, G_{y}, H_{y}, L_{y}, M_{y} and N_{y} parameters of the Hill 48 yield surface as suggested by Wang *et al.* [7]:

$$F_{\mathrm{y}} = \frac{1}{2}\left(\frac{1}{{\sigma_{90}}^2} - \frac{1}{{\sigma_0}^2} + \frac{1}{{\sigma_{\mathrm{z}}}^2}\right){S_{y0}}^2 \quad (2)$$

$$G_{\mathrm{y}} = \frac{1}{2}\left(\frac{1}{{\sigma_0}^2} - \frac{1}{{\sigma_{90}}^2} + \frac{1}{{\sigma_{\mathrm{z}}}^2}\right){S_{y0}}^2 \quad (3)$$

$$H_y = \frac{1}{2}\left(\frac{1}{{\sigma_0}^2} + \frac{1}{{\sigma_{90}}^2} - \frac{1}{{\sigma_{\mathrm{z}}}^2}\right){S_{y0}}^2 \quad (4)$$

$$N_y = \left(\frac{2}{{\sigma_{45}}^2} - \frac{1}{2{\sigma_{\mathrm{z}}}^2}\right){S_{y0}}^2 \quad (5)$$

$$M_{\mathrm{y}} = L_{\mathrm{y}} = N_{\mathrm{y}} \quad (6\text{-}7)$$

The plastic potential Q was defined by:

$$Q = F_{\mathrm{p}}(\sigma_{22}-\sigma_{33})^2 + G_{\mathrm{p}}(\sigma_{33}-\sigma_{11})^2 + H_{\mathrm{p}}(\sigma_{11}-\sigma_{22})^2 + 2L_{\mathrm{p}}{\sigma_{23}}^2 + 2M_{\mathrm{p}}{\sigma_{31}}^2 + 2N_{\mathrm{p}}{\sigma_{12}}^2 - {S_{\mathrm{y}}}^2 \quad (8)$$

In order to include planar strain anisotropy, R-value parameters R_0, R_{45} and R_{90} were used according to Kami *et al.* [8] to determine F_{p}, G_{p}, H_{p}, L_{p}, M_{p} and N_{p} parameters of the Hill 48 plastic potential:

$$H_{\mathrm{p}} = \frac{R_0}{(R_0+1)} \quad (9)$$

$$F_{\mathrm{P}} = \frac{H_{\mathrm{p}}}{R_{90}} \quad (10)$$

$$G_{\mathrm{p}} = \frac{H_{\mathrm{p}}}{R_0} \quad (11)$$

$$N_{\mathrm{p}} = \frac{(R_0+R_{90})(2R_{45}+1)}{2R_{90}(R_0+1)} \quad (12)$$

$$M_{\mathrm{p}} = N_{\mathrm{p}} = \frac{3}{2} \quad (13\text{-}14)$$

The temperature and rate sensitivity was introduced by making the stress anisotropy parameters temperature and strain rate dependent ($\sigma_0(T,\dot{\varepsilon})$, $\sigma_{45}(T,\dot{\varepsilon})$ and $\sigma_{90}(T,\dot{\varepsilon})$) and the R-value parameters temperature dependent ($R_0(T)$, $R_{45}(T)$ and $R_{90}(T)$). The hardening curves were stored in a free table form separately for each experimental temperature and strain rate combination. Linear interpolation was used for strain and temperature dependence and logarithmic interpolation was used for strain rate dependence. The plasticity model was calibrated from hot tensile tests as described in D'Amours *et al.* [9].

3. Damage model

A phenomenological damage accumulation framework was adopted in this study to predict both plastic instability and fracture. The developed model was based on GISSMO [10] with added temperature and strain rate sensitivity. Two elemental scalar variables, *D* and *IM*, were introduced for fracture and instability risk accumulation respectively at every integration point. Both variables had critical value of 1.0 and initial value of $1x10^{-10}$. An increment of *D* was computed at every time step upon completion of plastic update using the following equation:

$$\Delta D = dx \left(\frac{\varepsilon_{\mathrm{p}}}{\varepsilon_{\mathrm{f}}(T,\dot{\varepsilon},\xi,\eta)}\right)^{(dx-1)} \left(\frac{\Delta\varepsilon_{\mathrm{p}}}{\varepsilon_{\mathrm{f}}(T,\dot{\varepsilon},\xi,\eta)}\right) \tag{15}$$

where ε_{p} and $\Delta\varepsilon_{\mathrm{p}}$ are the equivalent plastic strain and its increment, dx is the damage exponent, ε_{f} is the fracture strain that depends of the temperature *T*, the strain rate $\dot{\varepsilon}$, the stress triaxiality η and the Lode parameter ξ. The instability measure *IM*, was incremented using:

$$\Delta IM = dx \left(\frac{\varepsilon_{\mathrm{p}}}{\varepsilon_{\mathrm{i}}(T,\dot{\varepsilon})}\right)^{(dx-1)} \left(\frac{\Delta\varepsilon_{\mathrm{p}}}{\varepsilon_{\mathrm{i}}(T,\dot{\varepsilon})}\right) \tag{16}$$

where ε_{i} is the instability strain that depends of the temperature *T*, the strain rate $\dot{\varepsilon}$.

Stress coupling was implemented for the post-instability response (*IM* ≥ *1.0*) to insure a gradual decrease of load bearing capacity to 0 when the value of damage parameter *D* reaches unity. This was achieved by the following update to the uncoupled stress vector $\vec{\sigma}$:

$$\vec{\sigma}_{\mathrm{new}} = \left(1 - \left(\frac{D_{\mathrm{new}} - D_{\mathrm{ins}}}{1 - D_{\mathrm{ins}}}\right)^{fx}\right)\vec{\sigma} \tag{17}$$

where fx is the fade exponent for stress coupling and *D*ins is the value of *D* when the instability *IM* reaches the value of 1.0. The instability strain $\varepsilon_{\mathrm{i}}(T,\dot{\varepsilon})$ was determined directly from the hot tensile test results. Fracture surfaces $\varepsilon_{\mathrm{f}}(\xi,\eta)$ were assumed to have shape proposed by Bai et al. [11]:

$$\varepsilon_{\mathrm{f}} = \left(c_0\left(c_\xi^{\mathrm{s}} + \frac{\sqrt{3}}{2-\sqrt{3}}\left(c_\xi^{\mathrm{ax}} - c_\xi^{\mathrm{s}}\right)\left(\frac{1}{\cos\left(\frac{\xi\pi}{6}\right)} - 1\right)\right)\left(\sqrt{\frac{1+{c_1}^2}{3}}\cos\left(\frac{\xi\pi}{6}\right) + c_1\left(\eta + \frac{1}{3}\sin\left(\frac{\xi\pi}{6}\right)\right)\right)\right)^{-\frac{1}{n}} \tag{18}$$

$$c_\xi^{\mathrm{ax}} = \begin{cases} 1 \ for\ \xi \geq 0 \\ c_\xi^{\mathrm{c}}\ for\ \xi < 0 \end{cases} \tag{19}$$

where $c_\xi^{\mathrm{s}}(T,\dot{\varepsilon})$, $c0(T,\dot{\varepsilon})$, $c1(T,\dot{\varepsilon})$, $c_\xi^{\mathrm{c}}(T,\dot{\varepsilon})$, and $n(T,\dot{\varepsilon})$ are free parameters determined separately for each combination of temperature and strain rate by minimizing the difference between the experimental and simulation results for three loading paths (uniaxial, plane strain and biaxial) as described in D'Amours *et al.* in [9] and [12].

4. Cross-die test setup

An open-top cross-die test setup, shown in Figure 1, has been designed and fabricated for HTC calibration and validation tests. The die had a 3-pieces configuration with the cavity on top, and the punch with the binder on the bottom. While binder was necessary to control wrinkling, a clearance larger than the material thickness was kept between the die and the binder during the experiments to reduce premature temperature loss in the binder area of the blank. Square 178 x 178 mm blanks with thickness of 2 mm were used in the tests. Both surfaces of the blank were painted with flat black paint for thermal imaging and then covered with graphite for lubrication. A FLIR camera was positioned above the press as shown in Figure 1. The camera was capturing the distribution of the blank's upper surface temperature at a frequency of 10 Hz.

Figure 1. Cross die test setup developed for hot stamping with blank temperature measurements

5. Calibration of the interfacial contact heat transfer conductance

The HTC was calibrated by the inverse method. A selected cross-die experiment was modelled with an HTC vs contact pressure curve from prior research. Then the curve was adjusted to minimize the difference in temperature distribution between the model and the experiment. The final calibrated curve, presented in Figure 2, demonstrates rapidly increasing conductance with pressure which is coherent with previous research [2] [5]. Figure 3 shows the measured top surface temperature for the selected specimen at the beginning, after 1.5 s and at the end of the forming process (2.63 s). Predicted top surface temperatures for the same specimen are shown in Figure 4. Good agreement was observed between the simulation and the experiment.

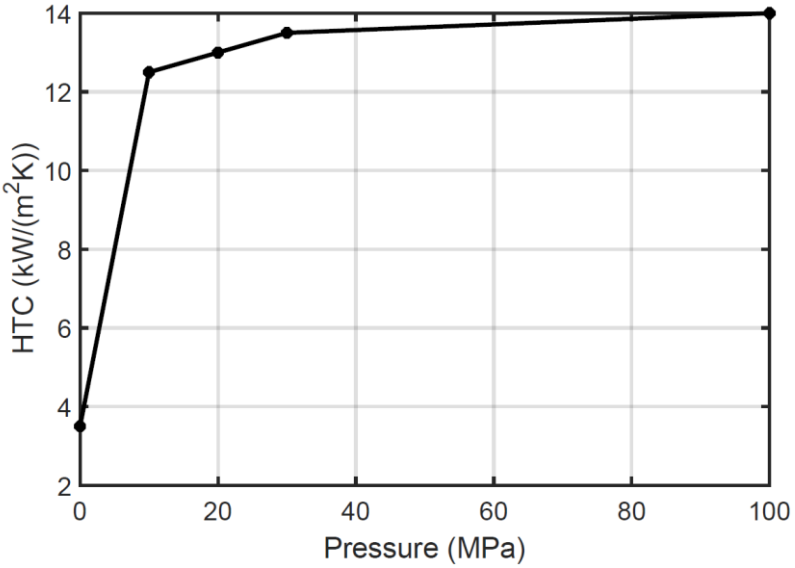

Figure 2. Calibrated HTC

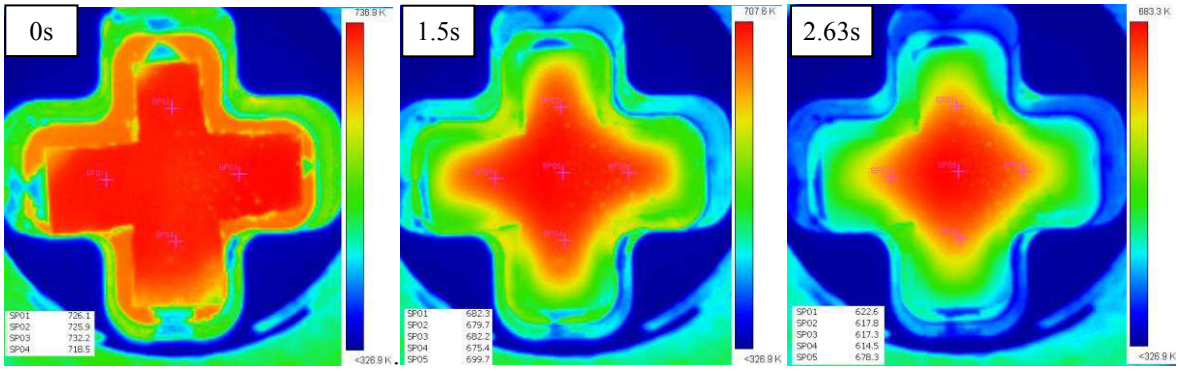

Figure 3. Measured top surface temperatures during hot stamping

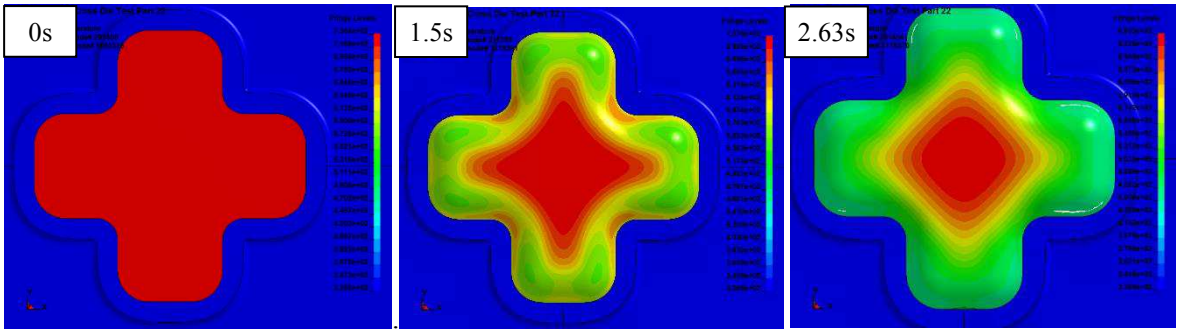

Figure 4. Predicted top surface temperatures during hot stamping

6. Validation

Validation tests were performed with various punch displacements and punch speeds to obtain a variety of post-form conditions including successful, necked, and fractured specimens. The punch was operated in displacement control with a smooth displacement profile. Figure 5 shows four hot stamped specimens with punch displacements varying from 24 mm to 26 mm and forming time from 1.5 to 2.63 sec. The modelling was performed using plane stress version of the user defined material model. Good agreement was observed between the simulation and experimental results. Figure 6 shows a fractured specimen and the predicted damage level.

Figure 5. Hot stamped cross specimens

7. Conclusion

This paper presented an overview of the material model developed for simulation of AA7075 aluminium sheet hot stamping. The model was based on the non-associated flow rule plasticity with Hill'48 yield function and plastic potential. It included isotropic hardening, phenomenological damage accumulation fracture and plastic instability criteria. The temperature and rate sensitivity were added by turning all model parameters and hardening into functions of temperature and rate. The presented approach demonstrated great potential in predicting both the plastic instability and fracture in hot forming. Additionally, it was shown that in-situ FLIR temperature measurements of the blank's surface temperature are really useful for the heat transfer conductance calibration. The HTC calibrated using the

inverse method demonstrated good accuracy in prediction of the temperature distribution during the hot stamping tests.

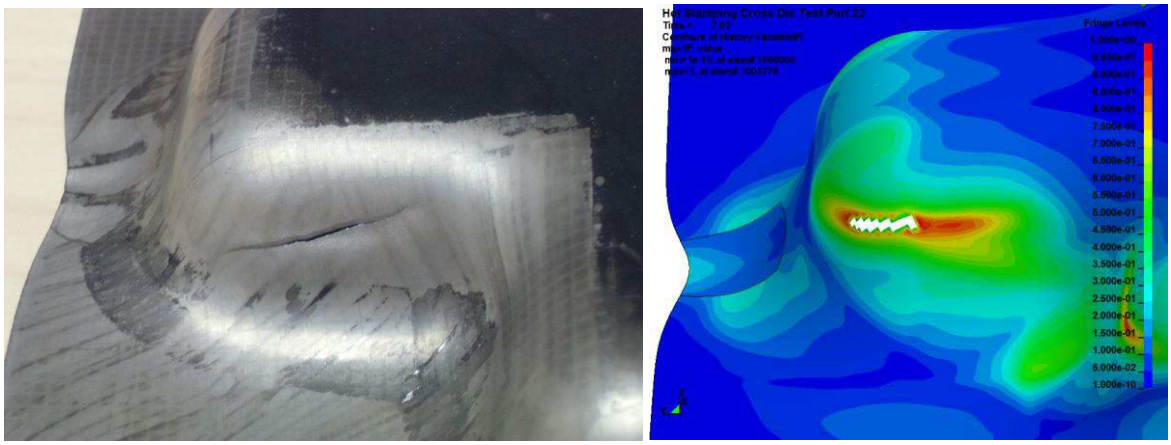

Figure 6. Hot stamped cross specimen with visible fracture (left) and the damage distribution predicted by the user material model (right)

References

[1] Harrison N R and Luckey S G 2014 Hot stamping of a B-pillar outer from high strength aluminum sheet AA7075 *SAE Int. J. Mater. Manuf.* **7** pp 567–73
[2] Ilinich A and Luckey S G 2014 On Modeling the hot stamping of high strength aluminum sheet *SAE Int.*
[3] Xiao W, Wang B and Zheng K 2017 An experimental and numerical investigation on the formability of AA7075 sheet in hot stamping condition *Int. J. Adv. Manuf. Technol.* **92** pp 3299–09
[4] Kumar M and Ross N G 2017 Investigations on the hot stamping of AW-7921-T4 alloy sheet *Adv. Mater. Sci. Eng.* pp 1–10
[5] Liu X, Ji K, El Fakir O, Liu J, Zhang Q and Wang L 2015 Determination of the interfacial heat transfer coefficient in the hot stamping of AA7075 *Matec Web of Conf.* **21**
[6] Hill R 1948 A Theory of the yielding and plastic flow of anisotropic metals *Math. Phys. Eng. Sci.* **193** pp 281–97
[7] Wang G, Qian X, Li X, Hou H, Liu Y and Lou Y 2014 A study on compressive anisotropy and nonassociated flow plasticity of the AZ31 magnesium alloy in hot rolling *Mathematical Problems in Engineering* **2014** pp 1–9
[8] Kami A, Bijan M D, Seyed ali S V, Dan-Sorin C and Banabic D 2014 Application of a GTN damage model to predict the fracture of metallic sheets subjected to deep-drawing. *P. Romanian Acad.* **15** pp 300-9
[9] D'Amours G and Ilinich A 2018 Plasticity and Damage Modeling of the AA7075 Aluminium Alloy for Hot Stamping *15th international LS-DYNA conference* paper submitted
[10] Andrade F X C, Feucht M, Haufe A and Neukamm F 2016 An incremental stress state dependent damage model for ductile failure prediction *Int. J. Fract.* **200** pp 127–50
[11] Bai Y and Wierzbicki T 2009 Application of extended Mohr–Coulomb criterion to ductile fracture *Int. J. Fract.* **161** pp.1–20
[12] D'Amours G and Ilinich A 2018 High temperature characterization and material model calibration for hot stamping of AA7075 aluminium sheet *J. Phys. Conf. Ser.* paper submitted